Characterization and Gas Adsorption Properties of Aluminum Methylphosphonates with Organically Lined Unidimensional Channels

Kazuyuki Maeda,* Yoshimichi Kiyozumi, and Fujio Mizukami

National Institute of Materials and Chemical Research, Higashi, Tsukuba, Ibaraki 305, Japan

Received: July 15, 1996; In Final Form: March 24, 1997[⊗]

Microporous aluminum methylphosphonates, AlMepO-α and -β, prepared by different procedures, were characterized mainly using ^{27}Al, ^{31}P, and ^{13}C MAS NMR, TG-DTA, and IR. The MAS NMR spectra were consistent with the crystal structures determined by the single-crystal X-ray structural analysis published previously. All the ^{31}P NMR signals were reasonably assigned using an assumed correlation between ^{31}P chemical shift and the mean Al−O−P angle around the phosphorus sites. Nitrogen adsorption isotherms of AlMepO-β degassed at elevated temperatures were of type I, while those of AlMepO-α gave two plateaus in the low relative pressure region. The stepwise adsorption was explained by a packing change of the adsorbate on adsorption. The pore diameter calculated from the maximum nitrogen adsorption capacity was consistent with adsorption of 2,2-dimethylpropane but was larger than the size expected from the crystal structure of both the compounds. The water vapor isotherm was type II in the low relative pressure region, confirming the hydrophobic nature for both compounds. AlMepO-α indicated no apparent adsorption of water into the channel, but AlMepO-β showed a sudden adsorption of water at $P/P_0 \approx 0.7$. The difference in the water vapor isotherms between the compounds was explained based on the relationship of the size of the water clusters formed and the shape of the adsorbent channel.

Introduction

Development of novel microporous crystalline material is of continuing interest because of the variety of applications such as catalysts, adsorbents, detergents, and ion-exchangers.[1,2] Most of the known crystalline molecular sieves possess an oxide framework with a (4;2)-3D net and a channel system as seen in zeolites and their related molecular sieves.[3] Also, chalcogenides[4] and nitrides[5] with channel structures are extensively studied. All these structures are purely inorganic wherein the channel walls are mainly composed of electronegative elements such as oxygen. The adsorption property of molecular sieves should be controlled by the character of the channel walls. We have tried to design the micropore walls with organic compounds that are covalently bonded to the oxide framework.

Organic compounds have great advantage in material engineering in terms of flexible and easily tailored structures. Layered oxides combined with organic compounds attracted much interest as molecularly engineered layered structures.[6] Such layered materials enable a two-dimensional array of organic molecules with specific physicochemical properties. Organic phosphonate is one of the most useful sources for building layered organic−inorganic composites[7,8] because of its structural diversity and relatively simple synthesis procedure. Compared with the layered phosphonate, organophosphonate with channel structure had been unexplored until very recently.[9−16] Many phosphates with channel structures, especially the aluminum phosphate ($AlPO_4$) molecular sieve family,[17,18] have been known. Generally, metal organophosphonates have a structural similarity with related metal phosphates.[19,20] From this clue we found two isomeric microporous aluminum methylphosphonates, designated AlMepO-α[11] and -β.[9,10]

The single-crystal structural analysis revealed that both frameworks (Figure 1) have the same composition, $Al_2(O_3PCH_3)_3$, and unidimensional channels lined with methyl groups along the *c*-axis.[10,11] These compounds contain 18-membered rings in the oxide framework. This large opening is comparable to channels of VPI-5[21] with a diameter of ca. 12−13 Å. A large space that enables adsorption of small adsorbates remains even though the channels are lined with methyl groups. According to the crystal structure, a cross section of the organically lined unidimensional channels is close to a regular triangle with a side of ca. 7.0 Å for both materials. Copper[13] and zinc[14] phosphonates reported by Bujoli et al. also contain similar organically lined unidimensional channels. Several phosphites have unidimensional channel structures lined with hydrogen atoms.[22−26] These phosphonates and phosphites, however, contain 12-membered rings at the largest, which will not allow intrusion of small adsorbates as large as nitrogen molecules. Thus, AlMepO-α and -β are the first molecular sieves belonging to a new category of material that may be designated as "organozeolite". Gas adsorption properties of materials containing such organo-lined channels is of much interest. Both the compounds can be prepared without any templating agent, which is essential for $AlPO_4$ synthesis. Detailed investigation on the optimum synthesis conditions are being published separately along with nonporous byproducts designated as AlMepO-ζ and -δ.[12,27] Use of certain acidic and neutral organic additives such as acetic acid and dioxane was effective for obtaining large crystals of AlMepO-β. The use of alcoholic solvents such as ethylene glycol and glycerol instead of water favored the formation of AlMepO-α. Properties of each compound are expected to be different depending upon the preparation procedure. In this article we report physicochemical characterization and adsorption properties of AlMepO-α and -β prepared through different procedures.

* To whom correspondence should be addressed. Address: Molecular Recognition Lab., Department of Surface Chemistry, National Institute of Materials and Chemical Research, 1-1 Higashi, Tsukuba, Ibaraki 305, Japan. Telephone: 298(54)4632 (Japan). Fax: 298(54)4709 (Japan). E-mail: maeda@nimc.go.jp.

[⊗] Abstract published in *Advance ACS Abstracts,* May 1, 1997.

S1089-5647(96)02112-8 CCC: $14.00 © 1997 American Chemical Society

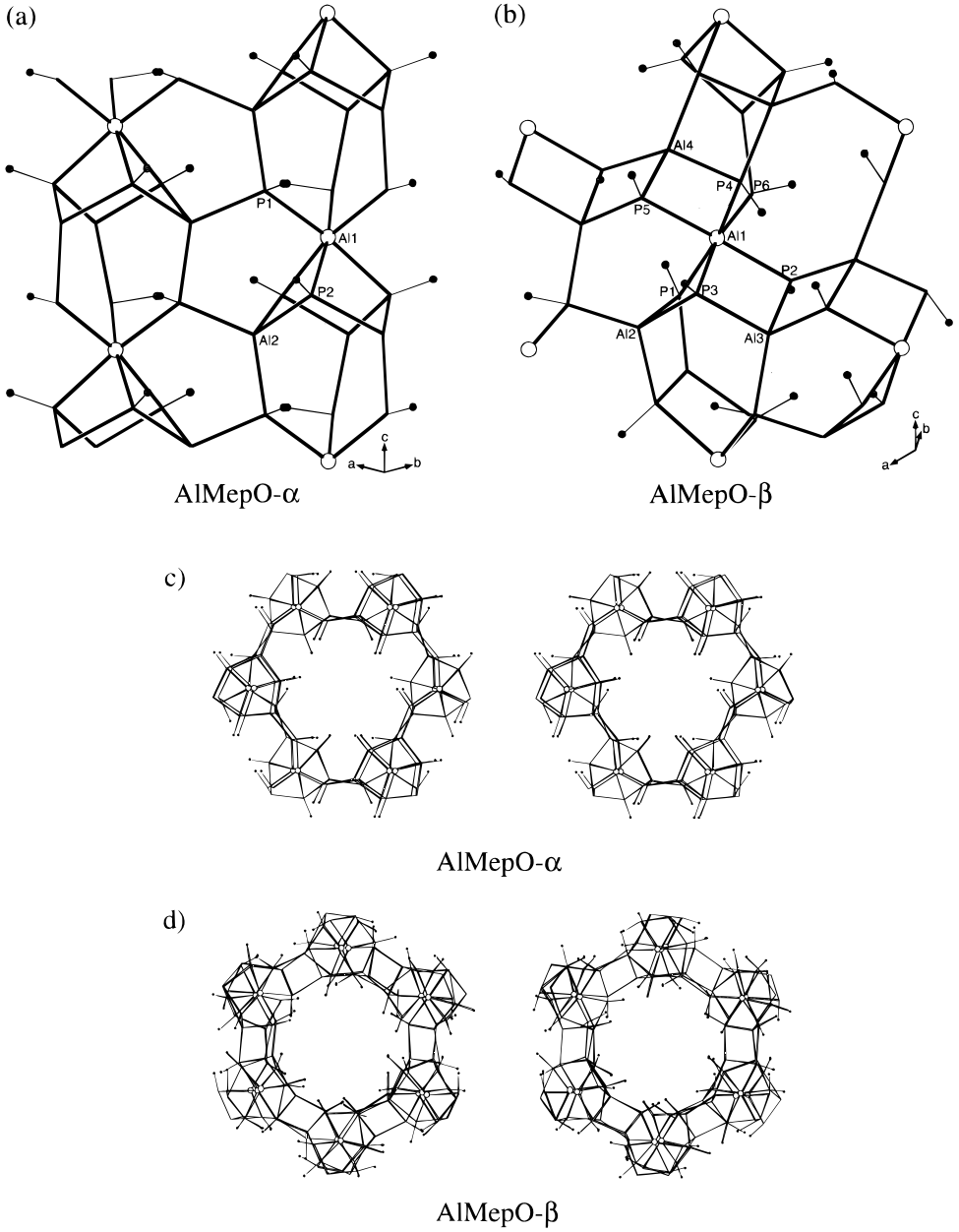

Figure 1. Framework structures viewed normal to [001] (a and b) and stereoplots viewed along [001][12] (c and d) of AlMepO-α (a and c) and AlMepO-*β* (b and d): open circle, Al_{Oh}; black circle, methyl group. Oxygen atoms are omitted.

Experimental Section

Materials. The aluminum source was pseudo-boehmite powder (PURAL SCF, Condea Chemie, 74.4 wt % Al_2O_3, 25.6 wt % water). Methylphosphonic acid (98%) was obtained from Aldrich. Other organic reagents were obtained from Tokyo Kasei. All reagents were used without further purification.

Synthesis of AlMepO-α. AlMepO-α was prepared by three different procedures outlined previously.[11,12] The samples were designated as α-NA, α-EG, and α-SC. The procedures are detailed below.

α-NA was prepared in a hydrothermal method with no additives. First, 0.685 g (10 mmol) of pseudo-boehmite powder was spread over the bottom of a 20 mL Teflon vessel. Next, 1.467 g (15 mmol) of methylphosphonic acid was added over the pseudo-boehmite powder . To this solid mixture, 6.72 g of water (400 mmol as total) was poured as gently as possible not to agitate the boehmite powder surface. The mixture was allowed to stand for 48 h without any agitation. The vessel was set in a stainless steel autoclave, and the mixture was hydrothermally treated at 433 K for 48 h under static conditions. The needle-like crystalline product was filtered, washed with water, and air-dried. The purest product so far obtained in this procedure contained ca. 90% of AlMepO-α and small amounts of AlMepO-*β* and -ζ. The total yield was 0.49 g (ca. 29%).

α-EG was prepared with ethylene glycol instead of water as solvent. In a 20 mL Teflon vessel 0.685 g (10 mmol) of pseudo-boehmite powder and 1.467 g (15 mmol) of methylphosphonic acid were dispersed in 20 g of ethylene glycol by stirring for 1 h. The additional procedures were the same as in the case of α-NA. The yield was 1.44 g (ca. 76%).

α-SC was prepared from a mixture away from the ideal stoichiometry. In a 20 mL Teflon vessel, 0.978 g (10 mmol) of methylphosphonic acid was placed over 0.685 g (10 mmol) of pseudo-boehmite powder layer, and 6.72 g of water (400 mmol as total) was poured into the vessel gently without agitation. This mixture was hydrothermally treated at 493 K for 48 h without aging before the hydrothermal reaction. The product contained traces of needle-like crystals floating in the

solution and a large amount of boehmite-derived solid lump on the bottom of the vessel. The needle crystals were carefully filtered, washed with water, and air-dried. Thus prepared α-SC proved to contain no AlMepO-*β*, whereas the yield was very low (<40 mg, 3% based on methylphosphonic acid). Single crystals of α-SC were previously used for the single-crystal X-ray diffraction measurement.[11] So far, we have not succeeded in obtaining α-SC on a larger scale.

Synthesis of AlMepO-*β*. AlMepO-*β* was prepared by using procedures outlined previously[9,10,12] with (*β*-DX) and without (*β*-NA) the addition of dioxane. In a 20 mL Teflon vessel 0.685 g (10 mmol) of pseudo-boehmite powder and 1.467 g (15 mmol) of methylphosphonic acid were dispersed in 6.72 g of water (400 mmol as total). The mixture was stirred at ambient temperature for 1 h. The suspension was hydrothermally treated at 433 K for 48 h. The solid product was filtered, thoroughly washed with water, and air-dried. The yield was 1.04 g (ca. 58%). A sample thus prepared with no additive is abbreviated as *β*-NA. The sample prepared by the same procedure as that for *β*-NA except for an addition of 15 mmol of dioxane to the starting mixture is abbreviated as *β*-DX. The yield was 1.77 g (ca. 94%). Single crystals thus prepared was previously used for the single-crystal X-ray diffraction measurement of AlMepO-*β*.[10]

Instrumentation. Analysis for carbon and hydrogen content was performed on an organic elemental analyzer (Carlo Erba, EA1108). Phosphorus and aluminum analysis were done on a ICP spectrometer (Thermo Jarrell Ash, IRIS/AP) after the samples were dissolved in aqua regia by heating. X-ray powder diffraction patterns (XRD) were measured at 303 K on a MAC Science MXP-18 diffractometer with Cu Kα radiation. Lattice constants of as-synthesized samples and ones degassed at 673 K for 10 h were calculated using 12−16 well-resolved diffraction peaks in the range $2\theta = 17-40$ referenced to a Si standard.

All the solid-state NMR measurements were performed using 4 mm zirconia rotors on a Bruker AMX-500 spectrometer equipped with a magic angle spinning (MAS) unit. The ^{13}C CP/MAS NMR spectra were recorded at 125.76 MHz with reference to an external glycine standard (176.46 ppm) with a contact time of 1 ms, a delay time of 10 s, and a spinning rate of 4 kHz. The ^{27}Al MAS NMR spectra were recorded at 130.32 MHz referenced to a 1 M aqueous solution of aluminum nitrate (0 ppm) with a spinning rate of 4−5 kHz, ca. 5° pulse, and a recycle delay of 1 s. The ^{31}P MAS NMR spectra were recorded at 202.46 MHz referenced to 85% phosphoric acid (0 ppm) with a spinning rate of 4−5 kHz, 20° pulse, and a recycle delay of 10 s.

Thermogravimetry−differential thermal analysis (TG−DTA) were performed on a MAC Science TG-DTA 2000 equipment both under a flow of dry air and under a flow of nitrogen at 100 mL/min. The samples were well crushed prior to the measurements. IR spectra were measured under air using a Hitachi 260-50 spectrometer using the KBr pellet method. Samples were degassed at 673 K. Diffuse reflectance infrared Fourier transform (DRIFT) spectra were taken on a Perkin-Elmer 1720X spectrometer. Samples were heated to 673 K under a flow of helium and measured in situ at ambient temperature.

All gas adsorption isotherms were measured volumetrically on an automated gas and vapor adsorption equipment. Adsorption isotherms of nitrogen at 77 K and of *n*-propane, 2-methylpropane, and 2,2-dimethylpropane at 273 K were measured on Bel-Japan Belsorp-36. Water adsorption isotherms were measured at 298 K on Bel-Japan Belsorp-18. The samples were pulverized on an agate motor and evacuated with a turbo molecular pump ($<10^{-5}$ Torr) at 673 K for 10 h prior to the adsorption measurement unless specifically stated. Samples for the nitrogen adsorption were raised stepwise from 473 to 823 K and kept for 10 h at each temperature. The adsorption capacity of the degassed samples was calculated from the Dubinin−Radushkevich (DR) plot[28] using the isotherm data, assuming the density of the adsorbate being equal to that of the liquid adsorptive.

TABLE 1: Elemental Analysis of As-Synthesized AlMepO-α and -*β*

sample	C (%)	H (%)	Al (%)	P (%)	P/Al
α-NA	10.2	3.4	15.7	26.7	1.48
α-EG	11.2	3.4	14.2	24.5	1.50
β-NA	10.1	3.3	14.7	24.6	1.46
β-DX	13.5	3.2	14.3	24.7	1.51
calculated for $Al_2(CH_3PO_3)_3$	10.7	2.7	16.1	27.7	1.50
calculated for $Al_2(CH_3PO_3)_3 \cdot H_2O$	10.2	3.1	15.2	26.3	1.50

TABLE 2: Lattice Constants of As-Synthesized and Heat-Treated AlMepO-α and -*β*

	lattice constant			
	as-synthesized		degassed at 673 K	
sample	*a*	*c*	*a*	*c*
α-NA	14.015(2)	8.545(2)	14.004(1)	8.535(1)
α-EG	14.003(2)	8.536(2)	13.992(3)	8.532(4)
α-SC	14.010(1)	8.540(2)	13.983(3)	8.525(3)
β-NA	24.758(3)	25.362(6)	24.748(3)	25.369(7)
β-DX	24.665(2)	25.289(4)	24.757(3)	25.364(4)

Results and Discussion

Elemental Analysis and XRD. Elemental analysis results of as-synthesized samples are shown in Table 1. Mass composition of α-SC could not be determined owing to the low yield. The ideal composition of both materials should be $Al_2(CH_3PO_3)_3 \cdot nH_2O$ accompanied by an additional organic content for α-EG and *β*-DX . Samples prepared without organic additive tend to deviate from the ideal P/Al ratio of 1.5. Carbon content of α-EG is slightly higher than those of the samples without additives. A composition of $Al_2(CH_3PO_3)_3(H_2O)_{0.6}$-$(C_4H_8O_2)_{0.3}$ can be estimated for *β*-DX according to the elemental analysis. Water content of the samples was estimated for $n = 0-2$ in the above-mentioned formula. It may vary depending on the drying process or even on humidity as revealed by water vapor adsorption results described later.

The highly crystalline nature of all the products has been confirmed from SEM images and XRD patterns.[12] Both products, AlMepO-α and -*β*, were needle-like crystals irrespective of the preparation procedures. The mean size of the crystals depended on the preparation procedure. For AlMepO-*β*, without additive (*β*-NA) the crystal dimensions were ca. 30−300 *μ*m in length and ca. 5−15 *μ*m in width. The crystal dimensions became ca. 10 times larger grown in aqueous dioxane (*β*-DX). For both α-NA and α-EG, crystal dimensions were in the range 30−300 *μ*m in length and 5−20 *μ*m in width.

According to XRD the samples were of single phase except α-NA and α-EG. α-NA contained small amounts of AlMepO-*β* and α-EG contained AlMepO-*δ* and -*ζ*. Lattice parameters of as-synthesized samples and of ones degassed at 673 K for 10 h are listed in Table 2. Differences in the lattice parameters among the as-synthesized AlMepO-α samples are small, while they are apparently shorter in *β*-DX than in *β*-NA. When the samples are degassed at 673 K, the lattice parameters of AlMepO-α tend to shorten, while those of *β*-DX become as large as those of *β*-NA. The lattice parameters of *β*-NA

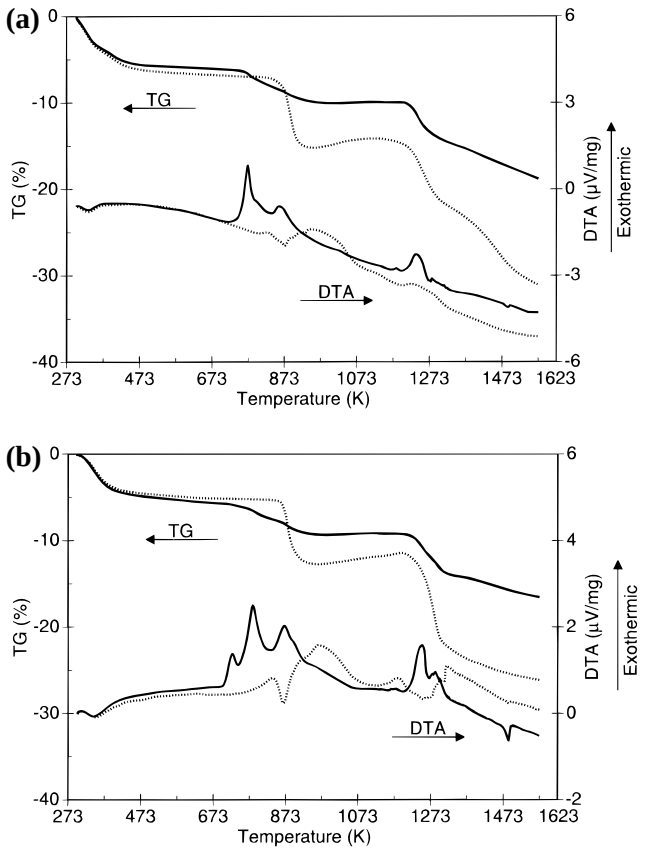

Figure 2. TG−DTA curves of as-synthesized samples under air (solid line) and nitrogen (dotted line): (a) α-EG; (b) *β*-NA.

remained unchanged. We interpret these results as follows. Although α-EG was synthesized in ethylene glycol with small water content, ethylene glycol is ready to be removed by washing with water. The ethylene glycol presumably remains mainly outside the channels at surface hydroxyl groups revealed by DRIFT spectra later. Dioxane tends to remain in as-synthesized *β*-DX by a selective uptake from water-rich reaction media because of its nonhydric nature, round shape, and appropriate size. Accordingly, ethylene glycol does not affect the lattice parameters of α-EG, while dioxane adsorbed in the channels induces the contraction of the *β*-DX lattice by hydrophobic interaction between methyl groups and the channel wall. However, water clusters formed in the hydrophobic channels can expand the lattice slightly. The expansion is reversed by removing the water.

Thermogravimetric Analyses and Thermal Stability. TG−DTA curves of α-EG and *β*-NA under a flow of dry air and nitrogen are shown in Figure 2. For α-EG, the initial weight loss below 473 K accompanied by an endothermic DTA peak at ca. 333 K is due to desorption of water from the unidimensional channels. The desorption at relatively low temperature supports the hydrophobic property of the channel. Little weight loss between the initial dehydration and decomposition of the methyl groups above 772 K revealed that most of the water and ethylene glycol have been eliminated below 473 K. The weight loss caused by the decomposition of the methyl groups occurs with two exothermic DTA peaks at 772 and 859 K under air. If methylphosphonate is completely oxidized to phosphate, the reaction should proceed as $Al_2(CH_3PO_3)_3 \rightarrow 2AlPO_4 \cdot {}^1/_2P_2O_5$. According to XRD, the product was amorphous at 823 K and consisted of small amounts of $AlPO_4$−tridymite of poor crystallinity at 923 K. Although the path should proceed ideally with 6.3% weight loss, the actual weight loss was 3.1% probably because of the carbonaceous component remaining in the product. Under nitrogen, 8.8% of the weight loss occurs with an endothermic DTA peak at 874 K. The larger weight loss under nitrogen should be due to decomposition of the methyl groups without oxidation of the phosphorus sites. According to XRD, α-EG was intact at 773 K and decomposed at 873 K under vacuum. An exothermic peak around 923 K is probably due to crystallization from amorphous $AlPO_4$ containing P_2O_5 to $AlPO_4$−tridymite. At higher temperatures the excessive P_2O_5 is gradually lost. Even at 1573 K the weight still continues to decrease and the crystallization into $AlPO_4$−tridymite is not complete. Phosphorus oxide is likely to be incorporated in the amorphous aluminum phosphate structure so that the elimination of the phosphorus oxide and the crystallization of $AlPO_4$ are hard to complete. Also, α-NA gave a curve very similar to that of α-EG.

AlMepO-*β* gave a curve fundamentally similar to that of AlMepO-α, and the thermal reaction path of AlMepO-*β* is probably similar to that of AlMepO-α. The dehydration occurred at 345 K. The methyl groups decompose with an endothermic peak at 866 K under nitrogen. Under air, the decomposition begins at lower temperature and proceeds with three exothermic peaks at 726, 782, and 869 K. The ^{31}P MAS NMR spectrum of AlMepO-*β* degassed at 873 K gave a new broad peak at −29.0 ppm, which can be assigned as being due to phosphate. This result reveals the transformation from methylphosphonate to phosphate under an inert atmosphere as well as under air. The TG curve of *β*-DX showed no plain part after the initial dehydration, and the following weight loss continues until the decomposition of methyl groups. This should be caused by slow desorption of dioxane occluded in the middle of the long unidimensional channels.

^{27}Al MAS NMR. Figure 3 shows the ^{27}Al MAS NMR spectra of as-synthesized AlMepO-α and -*β*. The purest AlMepO-α sample, α-SC, gives two main peaks at −21.3 and 42.0 ppm with an intensity ratio of 1:3. The former, assigned to the six-coordinate aluminum center (Al_{Oh}), appears at higher magnetic field than the octahedral aluminum center of typical $AlPO_4$ sieves with coordinated H_2O molecules.[29] The latter is assigned to four-coordinate aluminum centers (Al_{Th}).[29] Other AlMepO-α samples give similar spectra except for additional small peaks derived from byproducts. In the spectrum of α-NA an additional line at −17.6 ppm is attributed to AlMepO-*β*; in the spectrum of α-EG the small line at 14.3 ppm is derived from AlMepO-*δ*. According to our previous X-ray structural analysis using a twinned single-crystal corresponding to α-SC, the space group *P*3*c* gave a reasonable structural model, and the refinement led to a satisfactory convergence ($R_w = 0.046$).[11] The framework proved to contain only one Al_{Th} and one Al_{Oh} site (Figure 1a). Nevertheless, all AlMepO-α spectra give an additional Al_{Th} peak at 41.4−41.6 ppm with poor peak separation. So far, we have no clear explanation for the additional Al_{Th} peaks.

Sample *β*-DX gives an incompletely resolved Al_{Th} peak with three components at 43.0, 41.9, and 41.3 ppm and one Al_{Oh} peak at −17.7 ppm with an intensity ratio of 3:1. This result is consistent with the single-crystal analysis[10] revealing that AlMepO-*β* should have one Al_{Oh} and three independent Al_{Th} sites (Figure 1b). Sample *β*-NA gives two peaks at 41.3 and −17.5 ppm with an intensity ratio of 3:1. The broad and irregular shape with a bulge at low-field side of the Al_{Th} peak is caused by the overlapping of three peaks as in the case of *β*-DX.

An empirical linear correlation between mean Al−O−P angles around the aluminum centers and ^{27}Al chemical shifts is known for dense aluminophosphate polymorphs[30] and micro-

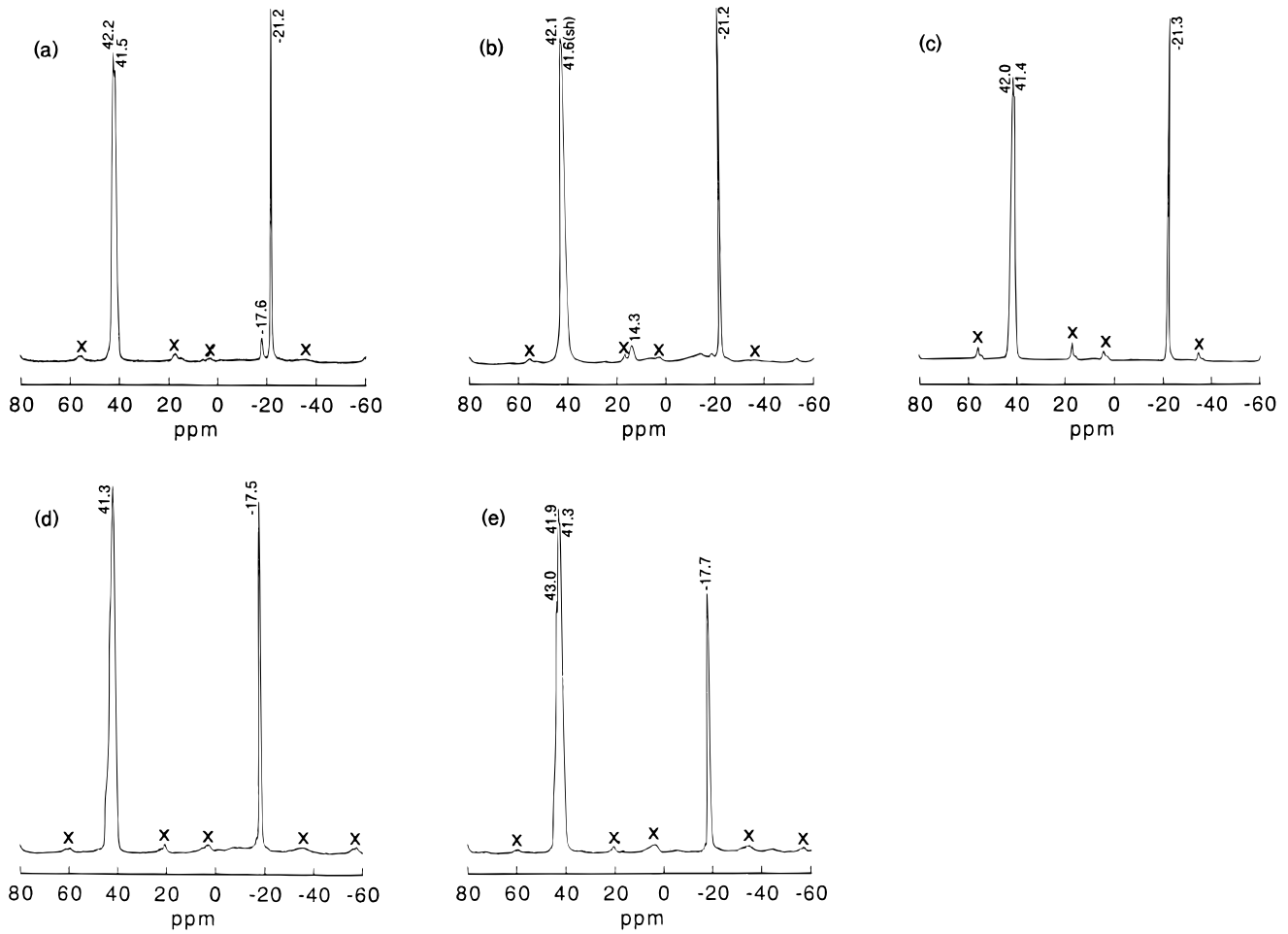

Figure 3. ^{27}Al MAS NMR of as-synthesized samples: (a) α-NA; (b) α-EG; (c) α-SC; (d) *β*-NA; (e) *β*-DX (X: sidebands).

TABLE 3: Mean Al−O−P Angles and ^{27}Al Chemical Shifts

	Al_{Oh}			Al_{Th}		
	site	mean Al−O−P angle (deg)	*δ* (ppm)	site	mean Al−O−P angle (deg)	*δ* (ppm)
α-SC	Al1	155.4(3)	−21.3	Al2	148.1(2)	42.0 (41.4[a])
β-DX	Al1	145.7(3)	−17.7	Al2	145.8(4)	
				Al3	147.2(4)	41.3, 41.9, 43.0
				Al4	143.8(4)	

[a] Shoulder.

porous $AlPO_4$ sieves.[31] Generally, the smaller mean Al−O−P angles tend to give the corresponding ^{27}Al signal at the lower magnetic field. Therefore, a similar correlation between the chemical shifts and the mean Al−O−P angle is expected also for aluminum phosphonates. The mean Al−O−P angles calculated for AlMepO-α and -*β* using the structural data and the corresponding ^{27}Al chemical shifts for α-EG and *β*-DX are listed in Table 3. The Al_{Oh} signal of AlMepO-α appears at higher magnetic field than that of AlMepO-*β* in which the mean Al−O−P angle around the aluminum center is smaller. The chemical shift difference among all four Al_{Th} included in both compounds is small probably because the mean Al−O−P angles are close. This result suggests that a correlation between ^{27}Al chemical shift and mean Al−O−P angle is valid for aluminum methylphosphonate as well as for $AlPO_4$.

^{31}P MAS NMR. Figure 4 shows the ^{31}P MAS NMR spectra of as-synthesized AlMepO-α and -*β*. Sample α-SC gives two sharp signals at 5.5 and 0.4 ppm, while *β*-DX gives five sharp signals at 14.7, 13.1, 10.9, 7.3, and 1.7 ppm. According to the single-crystal X-ray result, there are two and six crystallographically independent phosphorus sites included in AlMepO-α[11] and -*β*,[10] respectively. The peak at 1.7 ppm, which is twice as intense as the other peaks, should consist of two overlapping independent peaks. In the spectrum of α-NA, additional broad peaks at 13.6 and 9.9 ppm are derived from incompletely resolved signals of AlMepO-*β*. In the spectrum of α-EG, peaks at 12.9, 10.6, and 8.6 ppm are derived from AlMepO-*δ*. There is no difference in the positions of the peaks characteristic of AlMepO-α among the three samples despite the coexistence of other phases. However, all the signals of *β*-NA appear at slightly higher magnetic field compared to those of *β*-DX.

Also, ^{31}P chemical shifts are related to the mean Al−O−P angles around phosphorus centers in $AlPO_4$ and $AlPO_4$−hydrate systems.[30,32] There was no report on correlation between ^{31}P chemical shifts and mean Al−O−P angles for compounds other than phosphates. In the present AlMepO system the local small ring system around the phosphorus sites is supposed to dominate the local phosphorus environment because all the sites are equally connected to one Al_{Oh} and two Al_{Th} via oxygen atoms. Therefore, we tried to assign the ^{31}P signals of α-SC and *β*-DX. Table 4 lists experimentally determined Al−O−P angles around all the phosphorus sites of AlMepO-α and -*β* and the ^{31}P peak assignments. The size and number of the rings including each phosphorus site are also given in Table 4. For example, 4^26^1 indicates that the corresponding phosphorus site is included in two four-membered rings and one six-membered ring. AlMepO-α has 4^26^1 and 6^3 sites, and AlMepO-*β* has two 4^26^1, three 4^28^1, and one 6^28^1 sites. For convenience we classified the local small ring systems that appear in AlMepO compounds into three groups: 4^26^1, 4^28^1, and 6^2n^1 (6^3 and 6^28^1). Observed

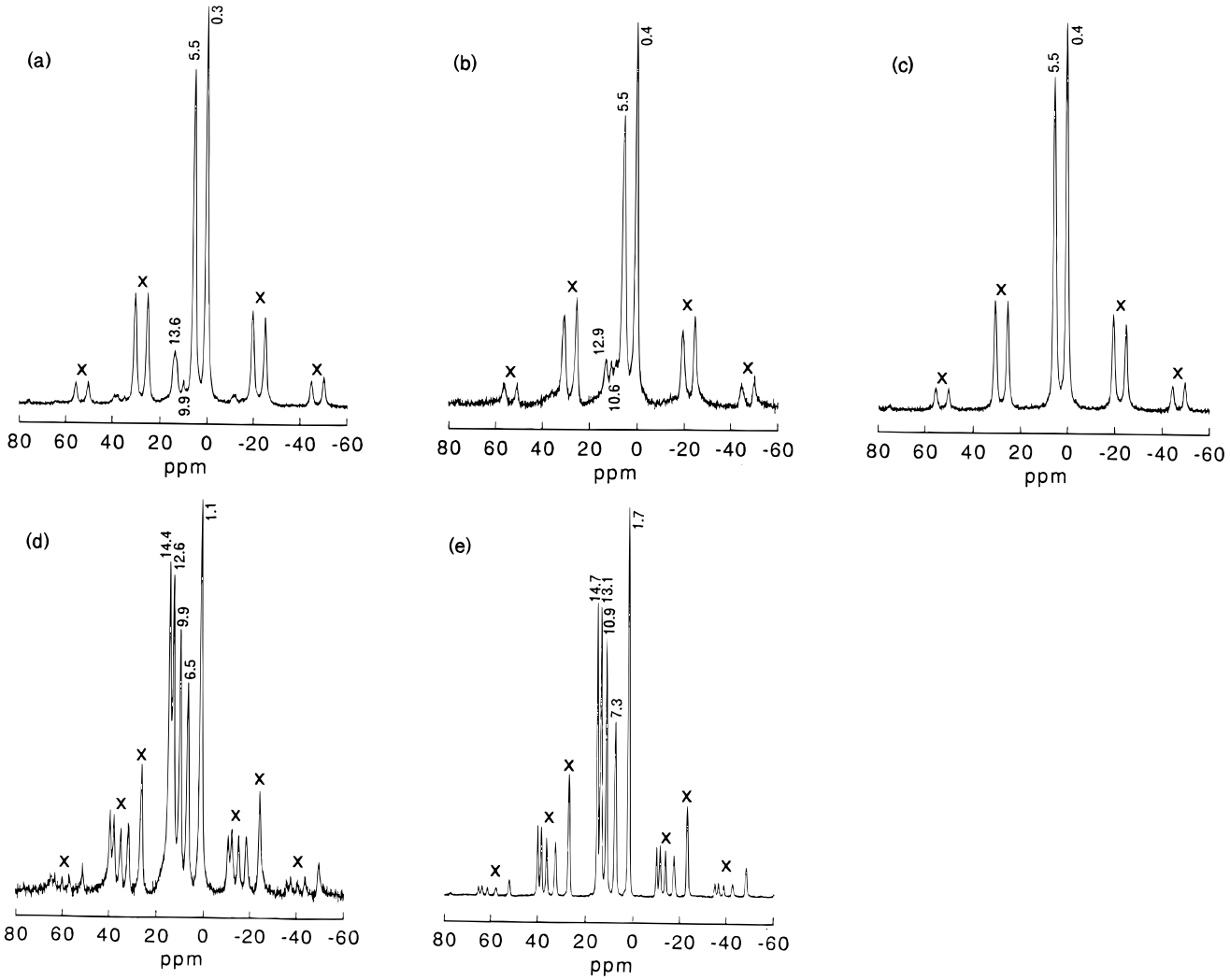

Figure 4. ^{31}P MAS NMR of as-synthesized samples: (a) α-NA; (b) α-EG; (c) α-SC; (d) *β*-NA; (e) *β*-DX (X: sidebands).

TABLE 4: Al−O−P Angles and Assigned ^{31}P Chemical Shifts

α-SC site	ring system	Al−O−P angles (deg) Al1	Al2	Al2′	mean Al−O−P angle (deg)	*δ* (ppm)
P1	6^3	150.2	145.7	149.2	148.4(2)	5.5
P2	4^26^1	160.6	146.1	151.2	152.6(2)	0.4

β-DX site	ring system	Al−O−P angles (deg) Al1	Al2	Al3	Al4	mean Al−O−P angle (deg)	*δ* (ppm)
P1	4^28^1	139.2	137.3		144.5	140.3(4)	14.7
P2	4^28^1	148.1		143.1	137.6	142.9(4)	10.9
P3	4^26^1	143.2	153.4	157.1		151.2(5)	1.7
P4	4^28^1	143.6	145.7		133.8	141.0(4)	13.1
P5	4^26^1	152.1		142.6	159.2	151.3(5)	1.7
P6	6^28^1	148.1	146.8	146.1		147.0(5)	7.3

^{31}P signals may also be separated into three groups; ^{31}P signals that appear at magnetic fields lower than 10 ppm, at middle field (5−8 ppm), and at fields higher than 2 ppm are abbreviated as LFS (low-field signal), MFS (middle), and HFS (high), respectively. It should be noted that AlMepO-α has neither LFS nor 4^28^1, while AlMepO-*β* has three LFS and 4^28^1. Similarly, the doubled intensity of HFS and two 4^26^1 are included in AlMepO-*β*, while single HFS and one 4^26^1 are included in AlMepO-α. It should also be noted that the calculated mean Al−O−P angles apparently decrease in the order of $4^28^1 < 6^2n^1 < 4^26^1$. Accordingly, we tentatively assigned LFS to 4^28^1, MFS to 6^2n^1, and HFS to 4^26^1. Overlapping of two independent signals at 1.7 ppm can be accounted for by very close mean Al−O−P angles given by the P3 and P5 sites of AlMepO-*β*. Three LFS signals of AlMepO-*β* (P1, P2, and P4) are allocated based on the order of the mean Al−O−P angles (Table 4). Thus, all the assigned chemical shifts are plotted against the mean Al−O−P angles (Figure 5). This plot gives good linear correlation, although the data were taken from two different materials. The slope of the line, −1.13 ppm/

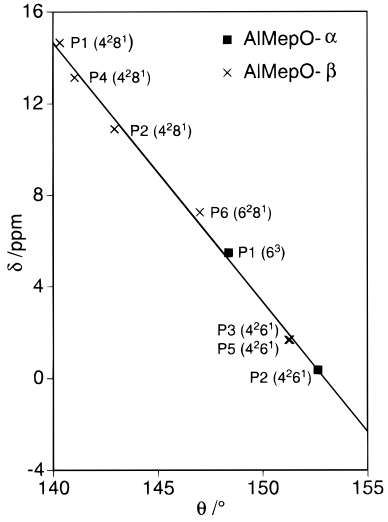

Figure 5. Correlation between mean P−O−Al angles and ^{31}P MAS NMR chemical shifts of assigned signals.

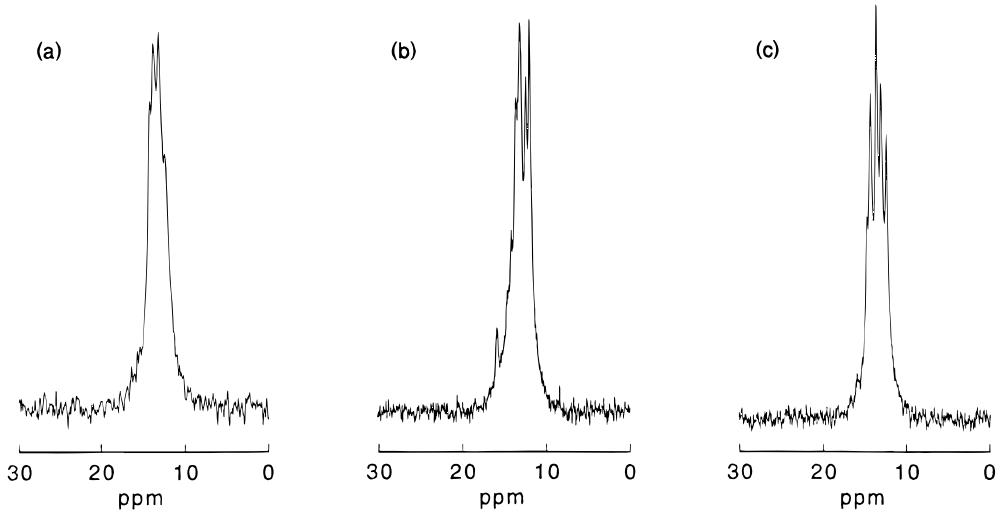

Figure 6. ^{13}C CP/MAS NMR of as-synthesized samples: (a) α-NA; (b) *β*-NA; (c) *β*-DX.

deg, is steeper than −0.51 ppm/deg[30] reported for aluminum phosphate. The low magnetic field drift of ^{31}P signals in *β*-DX compared with *β*-NA is explained by the decrease of mean Al−O−P angles due to the lattice contraction. This is supported by the fact that no noticeable difference in ^{31}P shift occurred between both samples degassed at 673 K with almost the same lattice parameters. Thus, we have succeeded in a rational assignment based on the structural data.

^{13}C CP/MAS NMR. The ^{13}C CP/MAS NMR spectra of the as-synthesized samples are shown in Figure 6. Free methylphosphonic acid gives a doublet at 11.3 ppm [^1J(C,P) = 140 Hz]. As-synthesized α-SC of a pure AlMepO-α phase gives four peaks in the range 12.0−14.0 ppm, which correspond to two doublets. Two crystallographically independent phosphorus sites of AlMepO-α affect chemical shifts of the next carbon to give different chemical shifts, and each peak is also split by a coupling with the adjacent phosphorus center. The methyl moieties are intact because no other peaks were observed. Sample α-EG gives less separated peaks owing to impure phases and a small broad peak around 63.7 ppm derived from ethylene glycol that probably interacts with the surface hydroxyl groups. Clusters of incompletely resolved peaks around 11.9−16.0 ppm were observed in *β*-NA and *β*-DX. It is reasonable to observe a more complicated pattern than that of AlMepO-α because AlMepO-*β* has six independent phosphorus sites. Each peak appears at almost the same position but with different intensity ratios between both samples. For *β*-DX a sharp signal is observed at 67.6 ppm assigned to dioxane. The narrow signal suggests that dioxane molecules stay unrestrainedly in the channels. The fact that the single-crystal X-ray diffraction of *β*-DX could not fix dioxane coordinates[10] supports this assumption.

Infrared Absorption Spectra. Figure 7 shows infrared spectra of α-EG and *β*-NA degassed at 673 K. Both spectra give similar C−H stretchings and bendings resulting from the presence of methyl groups. The band at ∼1320 cm^{-1} is characteristic for phosphonate with a P−C bond.[33,34] Generally, $AlPO_4$ gives a broad intense band (1200−1000 cm^{-1}) composed of several overlapping peaks derived from T−O stretches.[35−37] Both α-EG and *β*-NA give two separate clusters of overlapping peaks around 1230−1170 and 1150−1050 cm^{-1}, which can be assigned to P−O and Al−O stretches, respectively. The separation of the peaks is due to shorter P−O bonds and longer Al_{Th}−O and Al_{Oh}−O bonds than those of $AlPO_4$. Peaks at ∼475 and ∼440 cm^{-1} are assigned to Al−O and P−O bendings. Similar spectra were obtained for α-NA and *β*-DX. AlMepO-α gives a band at ∼340 cm^{-1}, probably derived from pore structure,[38] while AlMepO-*β* gives no distinct peak in this region.

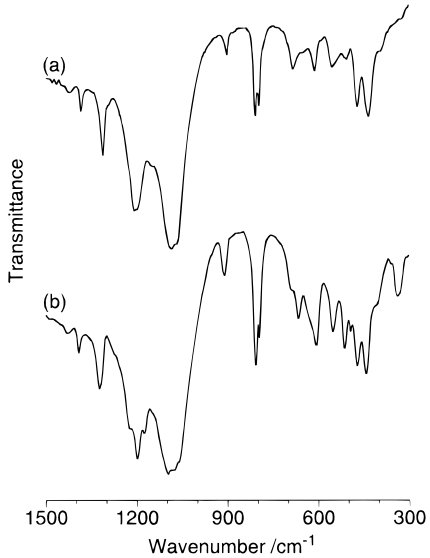

Figure 7. IR spectra of the structural region for samples degassed at 673 K for 10 h: (a) α-EG; (b) *β*-NA.

The DRIFT spectra of hydroxyl stretching vibration region for as-synthesized samples gave a broad band around 3000−3500 cm^{-1} derived from the physisorbed water. On heating at 673 K under a flow of helium, the intensity of this band decreased considerably because of desorption of water. As shown in Figure 8, α-EG gives four distinct absorption bands at 3637, 3729, 3829, and 3896 cm^{-1} and *β*-NA gives four bands almost at the same position even after heat treatment. The present compounds ideally should have neutral frameworks without any O−H groups. Actually, similar bands assigned to the stretching of terminal O−H groups located on the surface of crystals and/or at internal defect sites are often observed for $AlPO_4$ samples with neutral frameworks.[36] For $AlPO_4$-5 three absorption bands at 3680, 3740, and 3800 cm^{-1} were reported.[39] The bands at 3680 and 3800 cm^{-1} were assigned to the stretching of terminals P−OH and Al−OH, respectively.[40] The band at 3740 cm^{-1} was supposed to be assigned to Al−OH.[40] Therefore, the bands observed for AlMepO-α and -*β* can be attributed to the stretching of terminal O−H groups similar to $AlPO_4$'s. These compounds should have fundamentally three different types of terminal O−H groups: P−OH, Al_{Th}−OH,

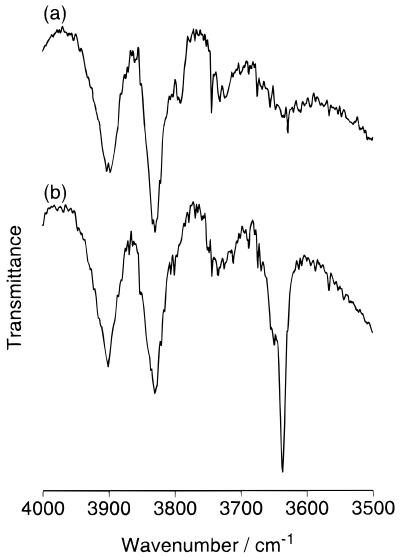

Figure 8. DRIFT spectra of the hydroxyl region for samples heated at 673 K: (a) α-EG; (b) *β*-NA.

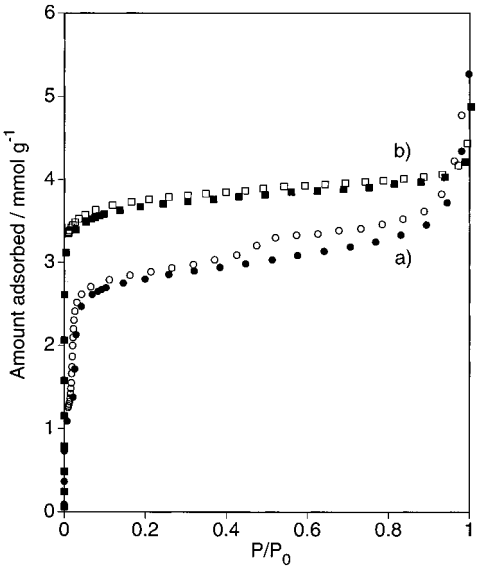

Figure 9. Nitrogen adsorption (solid symbols) and desorption (open symbols) isotherms on samples degassed at 673 K: (a) α-EG; (b) *β*-DX.

and Al_{Oh}−OH. The absorption band around 3900 cm^{-1} can be attributed to Al_{Oh}−OH because the longer mean distance of Al_{Oh}−O compared to Al_{Th}−O should increase the corresponding O−H stretching vibration frequency. The remaining three bands are assigned to P−OH and Al_{Th}−OH. Similar O−H bands in the region were observed also for α-NA and *β*-DX.

Nitrogen and Hydrocarbon Adsorption. Figure 9 shows nitrogen adsorption isotherms at 77 K of α-EG and *β*-DX degassed at 673 K for 10 h. The isotherm of AlMepO-*β* is typical of type I[41] based on IUPAC classification indicating microporous character. The small hysteresis loop, which does not close except at a very low-pressure region, is due to slow adsorption equilibrium in the unidimensional channels. Figure 10a shows nitrogen adsorption isotherms of *β*-DX successively degassed at elevated temperatures. The sample degassed at temperatures between 473 and 823 K gives type I isotherms. Nitrogen uptake increases with an increase in degassing temperature up to 773 K. At 773 K the sample gives the largest adsorption capacity of 0.134 mL g^{-1}, which is comparable with the reported capacity for $AlPO_4$-5 (0.146 mL g^{-1}) determined by oxygen adsorption.[42] Assuming a cylindrical channel, the channel diameter calculated from this maximum adsorption

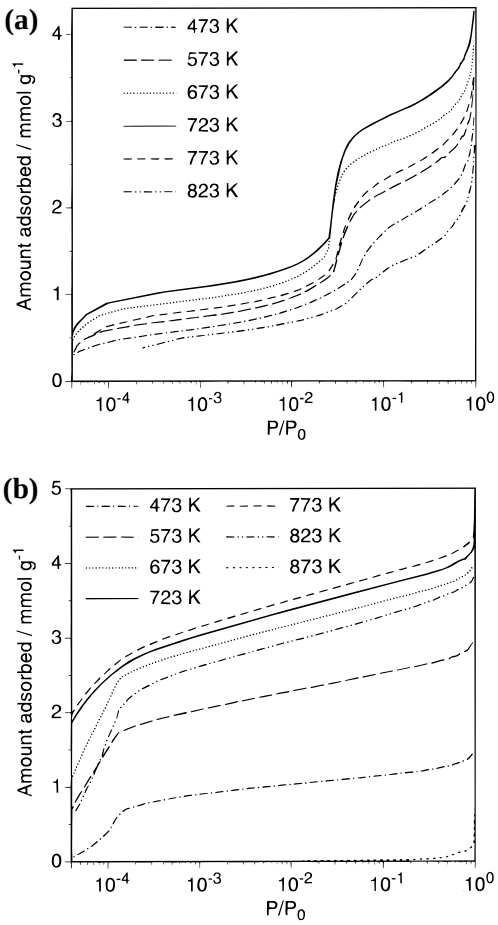

Figure 10. Nitrogen adsorption isotherms on samples successively degassed at elevated temperatures: (a) α-EG; (b) *β*-DX.

capacity is 6.7 Å, larger than the expected size from the crystal structure, suggesting flexibility of the channel wall or expansion of the lattice. The amount adsorbed begins to decrease at 823 K with sample color change. At 873 K the isotherm changes to type II,[41] revealing a loss of porosity. The black color of this sample shows decomposition of organic moieties. That is to say, decomposition of the methyl groups is accompanied by collapse of the porous structure and loss of crystallinity.

The isotherm of α-EG is also of type I at the low-pressure region. Unlike AlMepO-*β* there appears to be an additional transition in the relative pressure range $0.02 < P/P_0 < 0.03$ (Figure 9). This feature is not due to impure samples but is intrinsic for AlMepO-α because the pure AlMepO-α sample, α-SC, also gave an isotherm with two transitions fundamentally similar to those of α-EG and α-NA. A small amount of the sample, however, prevented quantitative measurements. The isotherms of AlMepO-α show a slight hysteresis, which does not close except at the low-pressure region. The isotherms also contain a small amount of a type IV[41] component with a hysteresis loop, probably due to nonporous byproducts or mesopores derived from crystal interstices of AlMepO-α. All the isotherms of α-EG degassed at temperatures ranging from 473 to 873 K have a pronounced second transition (Figure 10b). At higher degassing temperature up to 723 K the adsorption capacity increases; the second transition becomes clearer with a shift to a lower relative pressure region. Degassing at temperatures higher than 723 K causes a loss of porosity, and the second transition becomes slightly ambiguous. It is notable that the ratio of the amount absorbed at the second transition to that of the first transition is almost constant (2.1−2.5) irrespective of degassing temperatures. This suggests that there is no

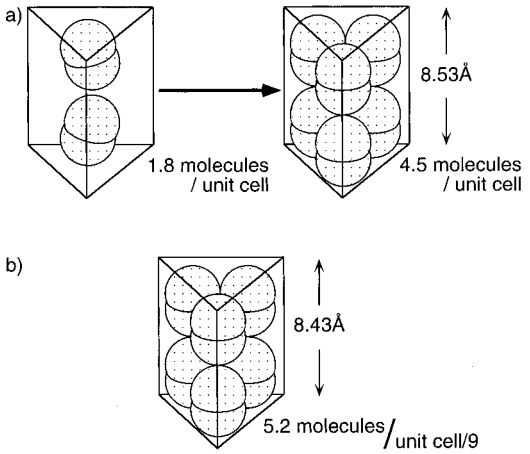

Figure 11. Nitrogen molecule packing models in AlMepO-α (a) and -β (b).

specific site for preferential adsorption in the channels of AlMepO-α.

As far as we know, the only comparable nitrogen adsorption isotherms with two plateaus in the low-pressure region are the ones reported by Müller and Ungar for large HZSM-5 crystals of uniform size.[43] These isotherms had the pronounced second transition with a hysteresis loop in the range $0.1 < P/P_0 < 0.15$. Similar isotherms with less distinct steps were also reported for less crystalline silicalite-1.[44] The two plateaus were assumed to be caused by a different packing of the adsorbed nitrogen in the zeolite. They pointed out that the ratio of the calculated amount adsorbed at both plateaus corresponded to the ratio of the density of liquid to that of solid nitrogen. Such a phase transition was also supported by low-temperature microcalorimetry results.[45] The adsorption isotherm of *p*-xylene on HZSM-5 at 343 K possessed two plateaus—similar to ours—with hysteresis in the range $0.02 < P/P_0 < 0.04$.[46] This was explained by a solid-phase change from 4 to 6.5 molecules of *p*-xylene per unit cell of ZSM-5. Besides ZSM-5, a smooth second transition in the range $0.01 < P/P_0 < 0.05$ was reported for an argon adsorption isotherm on VPI-5 at liquid argon temperature.[36]

At present we interpret the isotherm of AlMepO-α with two plateaus based on a packing change of adsorbed nitrogen molecules as shown in Figure 11. AlMepO-α and -β contain one and three channels per unit cell, respectively. The *c*-axis of AlMepO-β is nearly 3 times as long as that of AlMepO-α. Thus, it is possible to compare the number of nitrogen molecules adsorbed in a channel of the same length by taking a ninth of the unit cell of AlMepO-β compared with that of AlMepO-α. The maximum number of nitrogen molecules adsorbed in a channel of α-EG degassed at 723 K per unit cell is calculated to be 1.8 at the first plateau and 4.5 at the second one. In the same way, the maximum number of nitrogen molecules for β-DX degassed at 773 K per one-ninth of the unit cell is calculated to be 5.2. Because AlMepO-α and -β contain only six-membered rings and elliptical eight-membered rings at the largest, adsorption of nitrogen molecules should be confined to the main channels. Considering the width (3.0 Å) and length (4.1 Å) of a diatomic nitrogen molecule,[47] inclusion of ca. six nitrogen molecules into a unit cell needs very dense packing. The space of the approximately triangular prism-shaped channels in AlMepO-β should be effectively filled by locating nitrogen molecules as illustrated in a proposed packing model (Figure 11b). AlMepO-α also should allow a similar dense packing of nitrogen molecules. The smaller adsorption capacity of α-EG compared to β-DX may be caused by nonporous impurities.

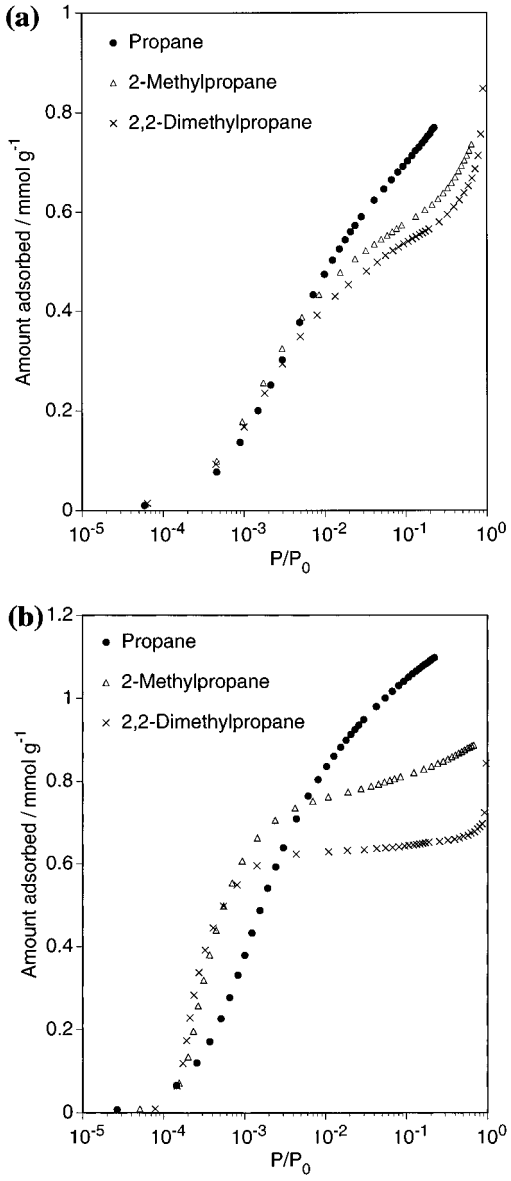

Figure 12. Hydrocarbon gas adsorption isotherms on samples degassed at 673 K: (a) α-EG; (b) β-DX.

Moreover, the difficulty in taking such a dense nitrogen packing is expected because AlMepO-α has more acute corners of the triangle than AlMepO-β according to the structural drawings. Therefore, nitrogen molecules may take a loose packing arrangement in the channels of AlMepO-α in the low relative pressure region (Figure 11a). Weak adsorbate−channel wall interaction compared to typical microporous oxides should favor such a packing transformation.

All the propane, 2-methylpropane, and 2,2-dimethylpropane adsorption isotherms on both adsorbents at 273 K are of type I (Figure 12). Adsorption of 2,2-dimethylpropane—kinetic diameter of 6.2 Å[47]—into the channels of both compounds is consistent with the channel diameters estimated from the nitrogen adsorption capacities. Adsorption capacity of the samples calculated from the DR plot for different adsorbates is listed in Table 5. Adsorption capacities for the hydrocarbons smaller than those for nitrogen indicates that the triangular channels prevent effective packing of adsorbates.

The adsorption capacities of both α-NA and β-NA are smaller than those of α-EG and β-DX for all the probe molecules, even though good crystallinity was confirmed by SEM and XRD. The low adsorption capacities are elucidated by blockage of unidimensional channels with a small amount of extraframework

TABLE 5: Adsorption Capacity of AlMepO-α and -β Calculated from the DR Plot

adsorbate	H_2O	N_2	C_3H_8	$CH(CH_3)_3$	$C(CH_3)_4$
kinetic diameter (Å)	2.65	3.64	4.3	5.0	6.2
pore volume (mL/g)					
α-NA		0.080	0.048	0.047	0.045
α-EG	(0.078)[a]	0.103	0.067	0.066	0.070
β-NA		0.068	0.048	0.044	0.035
β-DX	0.211[b]	0.124	0.094	0.087	0.077

[a] Calculated from the adsorbed amount at $P/P_0 = 0.97$. [b] Calculated from the adsorbed amount between $P/P_0 = 0.5$ and 0.7.

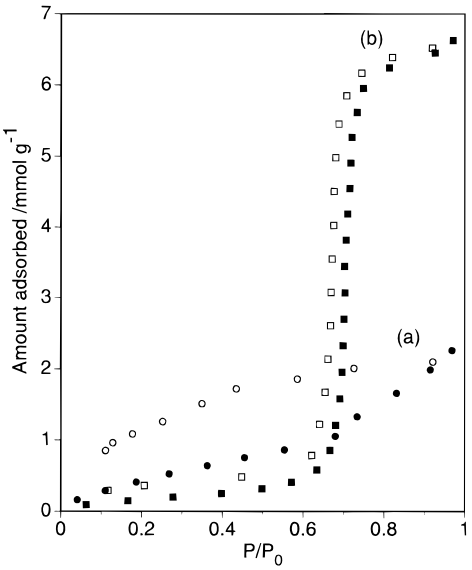

Figure 13. Adsorption (solid symbols) and desorption (open symbols) isotherms of water vapor on samples degassed at 673 K: (a) α-EG; (b) β-DX.

aluminum and/or methylphosphonate-derived components. As described above, large deviation from the ideal P/Al ratio (1.5) was observed for both the samples prepared without additives by ICP. This suggests the existence of extraframework components, although no ^{27}Al or ^{31}P MAS NMR signal was detectable. In the course of the hydrothermal reaction small aluminate and/or methylphosphonate species dissolving in the reaction solution should play an important role in the framework formation. Use of organic additives or solvents will reduce these species that remain in the unidimensional channels after the framework formation.

Water Vapor Adsorption. The water vapor adsorption isotherm of α-EG at 298 K (Figure 13a) is of type II, indicating the hydrophobic nature of the material. The large hysteresis loop does not close even at the lowest relative pressure because of the water trapped by the terminal hydroxyl groups on the crystal surface as revealed by the DRIFT spectra. The adsorption capacity estimated from the adsorbed amount at $P/P_0 = 0.97$ is smaller (0.078 mL g^{-1}) than the nitrogen adsorption capacity, although the contribution of surface hydration, which should be considerably large as suggested by the hysteresis loop, is neglected. This suggests that no or little adsorption into the organo-lined channels occurs in AlMepO-α. On the other hand, the isotherm of β-DX (Figure 13b) is also of type II, revealing hydrophobic nature until $P/P_0 \approx 0.6$ and whereupon a steep rise at $P/P_0 \approx 0.7$ followed by saturation at $P/P_0 \approx 0.8$ was observed. The hysteresis that does not close completely except at low relative pressure region is explained by surface hydration as well as α-EG. Such a steep rise and fall at the high relative pressure have not been known for conventional crystalline microporous materials.[36,41] Similar types can be found in certain microporous carbons,[48] although the shape of the micropore should be completely different. We try to explain this phenomenon and the difference between AlMepO-α and -β based on the interaction between the hydrophobic channel walls and adsorbate. The steep rise in the adsorption isotherm is not due to capillary condensation but due to micropore filling of water. The inside walls of the channels of both compounds should be hydrophobic, and only a small interaction between the channel walls and the adsorbates is expected compared to that in a microporous oxide. The higher relative pressure causes formation of larger water clusters, which enables a stronger interaction with the channel wall. Considerably higher relative pressure is required to form clusters large enough to be stabilized by intrusion into the channels of the present compounds. If such clusters are larger than the channel aperture, no stabilization on adsorption can occur. The acute triangular shape of AlMepO-α is probably less favorable for intrusion of spherical water clusters than the rounded shape of AlMepO-β. The adsorption capacity of β-DX for water vapor (0.211 mL g^{-1})—estimated from the difference of the adsorption amount at $P/P_0 = 0.5$ and 0.9—is far larger than the nitrogen adsorption capacity. This large adsorption capacity cannot be explained by considering only the adsorption into the main channels. Presumably, pockets between the methyl groups and the oxide skeleton are accessible to water molecules through six-memberd ring and elliptical eight-membered ring openings located on the channel wall.

Acknowledgment. We are grateful to Professor Katsumi Kaneko of Chiba University for valuable discussions and comments on gas adsorption results. We thank Dr. N. Padmakumar (NIMC) for helping us in the preparation of the manuscript.

References and Notes

(1) *Advanced Zeolite Science and Applications*; Jansen, J. C., Stöcker, M., Karge, H. G., Weitkamp, J., Eds.; Elsevier: Amsterdam, 1994, and references therein.

(2) Szostak, R. *Molecular Sieves*; Van Nostrand Reinhold: New York, 1989.

(3) Smith, V. *J. Chem. Rev.* **1988**, *88*, 149.

(4) Bedard, R. L.; Wilson, S. T.; Vail, L. D.; Bennett, J. M.; Flanigen, E. M. In *Zeolites: Facts, Figures, Future*; Jacobs, P. A., van Santen, R. A., Eds.; Elsevier: Amsterdam, 1989; p 375.

(5) Schnick, W. In *Zeolites and Related Microporous Materials: State of the Art 1994*; Weitkamp, J., Karge, H. G., Pfeifer, H., Hölderich, W., Eds.; Elsevier: Amsterdam, 1994; p 2221.

(6) Mallouk, T. E.; Lee, H. *J. Chem. Educ.* **1990**, *67*, 829.

(7) *Design of New Materials*; Clearfield, A., Cocke, D. A. Eds.; Plenum Press: New York, 1986.

(8) Thompson, M. E. *Chem. Mater.* **1994**, *6*, 1168.

(9) Maeda, K.; Kiyozumi, Y.; Mizukami, F. *Angew. Chem., Int. Ed. Engl.* **1994**, *33*, 2335.

(10) Maeda, K.; Akimoto, J.; Kiyozumi, Y.; Mizukami, F. *J. Chem. Soc., Chem. Commun.* **1995**, 1033.

(11) Maeda, K.; Akimoto, J.; Kiyozumi, Y.; Mizukami, F. *Angew. Chem., Int. Ed. Engl.* **1995**, *34*, 1199.

(12) Maeda, K.; Kiyozumi, Y.; Mizukami, F. In *Progress in Zeolite and Microporous Materials*; Chon, H., Ihm, S.-K., Uh, Y. S., Eds.; Elsevier: Amsterdam, 1997; p 197.

(13) Le Bideau, J.; Payen, C.; Palvadeau, P.; Bujoli, B. *Inorg. Chem.* **1994**, *33*, 4885.

(14) Drumel, S.; Janvier, P.; Deniaud, D.; Bujoli, B. *J. Chem. Soc., Chem. Commun.* **1995**, 1051.

(15) Poojary, D. M.; Grohol, D.; Clearfield, A. *Angew. Chem., Int. Ed. Engl.* **1995**, *34*, 1508.

(16) Poojary, D. M.; Cabeza, A.; Aranda, A. G.; Bruque, S.; Clearfield, A. *Inorg. Chem.* **1996**, *35*, 1468.

(17) Wilson, S. T.; Lok, B. M.; Messina, C. A.; Cannan, T. R.; Flanigen, T. M. *J. Am. Chem. Soc.* **1982**, *104*, 1146.

(18) Bennett, J. M.; Dytrych, W. J.; Pluth, J. J.; Richardson, J. W., Jr.; Smith, J. V. *Zeolites* **1986**, *6*, 349.

(19) Cao, G.; Hong, H.-G.; Mallouk, T. E. *Acc. Chem. Res* **1992**, *25*, 422.

(20) Zhang, Y. P.; Clearfield, A. *Inorg. Chem.* **1992**, *31*, 2821.
(21) Davis, M. E.; Saldarriaga, C.; Montes, C.; Garces, J.; Crowder, C. *Nature* **1988**, *331*, 698.
(22) Ortiz-Avila, C. Y.; Squattrito, P. J.; Shieh, M.; Clearfield, A. *Inorg. Chem.* **1989**, *28*, 2608.
(23) Sghyar, M.; Durand, J.; Cot, L.; Rafig, M. *Acta Crystallogr., Sect. C* **1991**, *47*, 2515.
(24) Morris, R. E.; Attfield, M. P.; Cheetham, A. K. *Acta Crystallogr., Sect. C* **1994**, *50*, 473.
(25) Marcos, M. D.; Amoros, P.; Le Bail, A. *J. Solid State Chem.* **1993**, *107*, 250.
(26) Attfield, M. P.; Morris, R. E.; Cheetham, A. K. *Acta Crystallogr., Sect. C* **1994**, *50*, 981.
(27) Maeda, K.; Hashiguchi, Y.; Kiyozumi, Y.; Mizukami, F. *Bull. Chem. Soc. Jpn.* **1997**, *70*, 345.
(28) Dubinin, M. M.; Radushkevich, L. V. *Proc. Acad. Sci. USSR* **1947**, *55*, 331.
(29) Blackwell, C. S.; Patton, R. L. *J. Phys. Chem.* **1984**, *88*, 6135.
(30) Müller, D.; Jahn, E.; Ladwig, G.; Haubenreisser, U. *Chem. Phys Lett.* **1984**, *109*, 332.
(31) Müller, D.; Jahn, E.; Fahlke, B.; Ladwig, G.; Haubenreisser, U. *Zeolites* **1985**, *5*, 53.
(32) Akporiaye, D.; Stöcker, M. *Zeolites* **1992**, *12*, 351.
(33) Harrison, W. T. A.; Dussack, L. L.; Vaughey, J. T.; Vogt, T.; Jacobson, A. J. *J. Mater. Chem.* **1996**, *6*, 81.
(34) Harrison, W. T. A.; Dussack, L. L.; Jacobson, A. J. *Inorg. Chem.* **1996**, *35*, 1461.
(35) van Nordstrand, R. A.; Santilli, D. S.; Zones, S. I. *ACS Symp. Ser.* **1988**, *368*, 236.
(36) Davis, M. E.; Montes, C.; Hathaway, P. E.; Arhancet, J. P.; Hasha, D. L.; Garces, J. M. *J. Am. Chem. Soc.* **1989**, *111*, 3919.
(37) Sierra de Saldarriaga, L.; Saldarriaga, C.; Davis, M. E. *J. Am. Chem. Soc.* **1987**, *109*, 2686.
(38) Flanigen, E. M.; Khatami, H.; Szymanski, H. A. *Adv. Chem. Ser.* **1971**, *101*, 201.
(39) Hedge, S. G.; Ratnasamy, P.; Kustov, L. M.; Kazansky, V. B. *Zeolites* **1988**, *8*, 137.
(40) Peri, J. B. *Discuss. Faraday Trans. Soc.* **1971**, 55.
(41) Gregg, S. J.; Sing, K. S. W. *Adsorption, Surface Area and Porosity*, 2nd ed.; Academic Press: London, 1982.
(42) Wilson, S. T.; Lok, B. M.; Messina, C. A.; Flanigen, E. M. *Proceedings of the Sixth International Zeolite Conference*; Olsen, D., Bisio, A., Eds.; Butterworth: Surrey, U.K., 1985; p 97.
(43) Müller, U.; Unger, K. K. In *Characterization of Porous Solids*; Unger, K. K., Rouquerol, J., Sing, K. S. W., Kral, H., Eds.; Elsevier: Amsterdam, 1988; p 101.
(44) Carrott, J. M. C.; Sing, K. S. W. *Chem. Ind. (London)* **1986**, 786.
(45) Müller, U.; Reichert, H.; Robens, E.; Unger, K. K.; Grillet, Y.; Rouquerol, F.; Rouquerol, J.; Pan, D; Mersmann, A. *Fresenius Z. Anal. Chem.* **1989**, *333*, 433.
(46) Olsen, D. H.; Kokotailo, G. T.; Lawton, S. L.; Meier, W. M. *J. Phys. Chem.* **1981**, *85*, 2238.
(47) Breck, D. W. *Zeolite Molecular Sieves*; Wiley: New York, 1974; p 636.
(48) Barton, S. S.; Evans, M. J. B.; MacDonald, J. A. F. *Carbon* **1991**, *29*, 1099.